# The chemical composition of the low-mass Galactic globular cluster NGC 6362[⋆]

D. Massari,[1,2,3]† A. Mucciarelli,[4,3]† E. Dalessandro,[3,4]† M. Bellazzini,[3] S. Cassisi,[5] G. Fiorentino,[3] R. A. Ibata,[6] C. Lardo[7] and M. Salaris[7]

[1]*University of Leiden, Leiden Observatory, NL-2300 RA Leiden, the Netherlands*
[2]*University of Groningen, Kapteyn Astronomical Institute, NL-9747 AD Groningen, the Netherlands*
[3]*INAF – Osservatorio Astronomico di Bologna, via Ranzani 1, I-40127, Bologna, Italy*
[4]*Dipartimento di Fisica e Astronomia, Università degli Studi di Bologna, v.le Berti Pichat 6/2, I-40127, Bologna, Italy*
[5]*INAF-Osservatorio Astronomico di Teramo, Via M. Maggini, I-64100 Teramo, Italy*
[6]*Observatoire astronomique de Strasbourg, Université de Strasbourg, CNRS, UMR 7550, 11 rue de l'Université, F-67000 Strasbourg, France*
[7]*Astrophysics Research Institute, Liverpool John Moores University, IC2, Liverpool Science Park, 146 Brownlow Hill, Liverpool L3 5RF, UK*

## ABSTRACT

We present chemical abundances for 17 elements in a sample of 11 red giant branch stars in NGC 6362 from UVES spectra. NGC 6362 is one of the least massive globulars where multiple populations have been detected, yet its detailed chemical composition has not been investigated so far. NGC 6362 turns out to be a metal-intermediate ([Fe/H] = −1.07 ± 0.01 dex) cluster, with its $\alpha$-peak and Fe-peak elements content compatible with that observed in clusters with similar metallicity. It also displays an enhancement in its s-process element abundances. Among the light elements involved in the multiple populations phenomenon, only [Na/Fe] shows star-to-star variations, while [Al/Fe] and [Mg/Fe] do not show any evidence for abundance spreads. A differential comparison with M4, a globular cluster with similar mass and metallicity, reveals that the two clusters share the same chemical composition. This finding suggests that NGC 6362 is indeed a regular cluster, formed from gas that has experienced the same chemical enrichment of other clusters with similar metallicity.

**Key words:** techniques: spectroscopic – stars: abundances – globular clusters: individual: (NGC 6362).

## 1 INTRODUCTION

With ages of the order of 12 mm 13 Gyr, globular clusters (GCs) are thought to be among the first stellar systems formed at early epochs in the Local Group. Thanks to the general homogeneity in terms of age and chemical composition of their stars, GCs have been used for decades as ideal tracers of the chemistry of their environments, allowing us to reconstruct the chemical enrichment history and the age–metallicity relation of their host galaxies.

The current picture of GC formation and evolution moves away from the traditional paradigm of GCs as simple stellar population (see for instance, the seminal paper by Renzini & Buzzoni 1986), according to which all the stars in a GC share the same initial chemical abundances for all the chemical elements. In fact, the recent discoveries of multiple sequences in GC colour–magnitude diagrams

(CMDs; see e.g. Piotto 2009; Piotto et al. 2015) and of star-to-star variations in the chemical abundances of some light elements (like C, N, Na, O, Mg, Al; see e.g. Gratton, Carretta & Bragaglia 2012, and references therein) demonstrate that such systems are indeed much more complex. Multiple populations (MPs) are ubiquitous in all GCs studied so far, both in the Galactic (see for example, Carretta et al. 2009; Gratton et al. 2012; Piotto et al. 2015) and extra-Galactic (Mucciarelli et al. 2009; Dalessandro et al. 2016) environment. Since this chemical pattern has been observed in stars at all the evolutionary stages (Gratton, Sneden & Carretta 2004; Milone et al. 2012), it cannot be explained in terms of internal mixing but it should have been imprinted in stars at formation. Several scenarios interpret the photometric and spectroscopic evidence in terms of different generations of stars, with a first generation polluting the gas out of which second generation of stars formed with the products of their internal evolution. A number of candidate polluters have been proposed (see Renzini et al. 2015 for a comprehensive review), namely, asymptotic giant branch stars (D'Ercole et al. 2008), fast-rotating massive stars (Decressin et al. 2007), massive binaries (de Mink et al. 2009) and supermassive stars (Denissenkov

**Table 1.** Fundamental properties of NGC 6362.

| NGC 6362 | |
|---|---|
| Right ascension (h:m:s) | 17:31:54.99 |
| Declination (°:′:″) | −67:02:54.0 |
| Distance (kpc) | 7.6 |
| $r_h$ (arcmin) | 2.5 |
| Mass ( $M_\odot$ ) | $5.3 \times 10^4$ |
| [Fe/H] (dex) | −1.07 |

*Note.* Position (Goldsbury et al. 2010), distance (Harris 1996), half-light radius and mass (Dalessandro et al. 2014) and metallicity (this work) of NGC 6362.

& Hartwick 2014). Alternative scenarios have been proposed as well, where low-mass stars accrete the polluted material during the pre-main-sequence phase to give rise to a chemically peculiar population of stars, which is coeval to that with pristine composition (Bastian et al. 2013).

The abundance spreads typical of MPs involve only a few light elements. For most of the elements (in particular $\alpha$-elements like Si, Ca and Ti, iron-peak and neutron-capture elements), the stars in a typical GC exhibit a remarkable level of internal homogeneity, thus suggesting that the abundances of these elements in GCs can be used to trace the chemical composition of the gas from which the cluster formed. Therefore, the investigation through high-resolution spectroscopy of the chemistry of poorly (or not yet) studied clusters is crucial to understand the chemical evolution of the Galactic halo (see e.g. Pritzl, Venn & Irwin 2005; Mészáros et al. 2015) and to identify, through the chemical tagging, clusters that likely originated in extragalactic environments (Mucciarelli et al. 2013a; Muñoz, Geisler & Villanova 2013; Villanova et al. 2013; Carretta et al. 2014; Marino et al. 2015).

In this paper, we present the first detailed chemical study of NGC 6362, an intermediate metallicity cluster that belongs to the low-mass tail of the GC mass distribution, with a mass of only $5 \times 10^4\,M_\odot$ (Dalessandro et al. 2014). We list cluster fundamental properties in Table 1, along with other useful information. Mucciarelli et al. (2016) first measured its iron content ([Fe/H] = –1.09 ± 0.01 dex) by analysing 160 giant stars observed with FLAMES at the Very Large Telescope. They also found a bimodal [Na/Fe] distribution, which makes NGC 6362 one of the least massive clusters where MPs have been detected. The peculiar radial distribution of its stars, with both first and second populations being completely mixed out to several hal-light radii, has been interpreted by Dalessandro et al. (2014) as the result of heavy mass-loss due to long-term dynamical evolution. Such a claim is also supported by the quite shallow present-day mass function observed for this cluster in Paust et al. (2010). Thus, it would be extremely interesting to investigate whether it also shows other exceptional chemical features or it follows the general trends observed for standard GCs in the Milky Way with MPs. To this end, we here present a detailed chemical analysis of 11 members in NGC 6362.

The paper is organized as follows. The data set analysed in this work is described in Section 2, while the details of the chemical analysis are discussed in Section 3. We present the results of this study in Section 4 and we finally discuss them in Section 5.

## 2  OBSERVATIONS AND DATA REDUCTION

The data set analysed in this work was acquired under the programmes 093.D-0618(A) and 097.D-0325(A), PI: Dalessandro, with the FLAMES spectrograph (Pasquini et al. 2002) at the
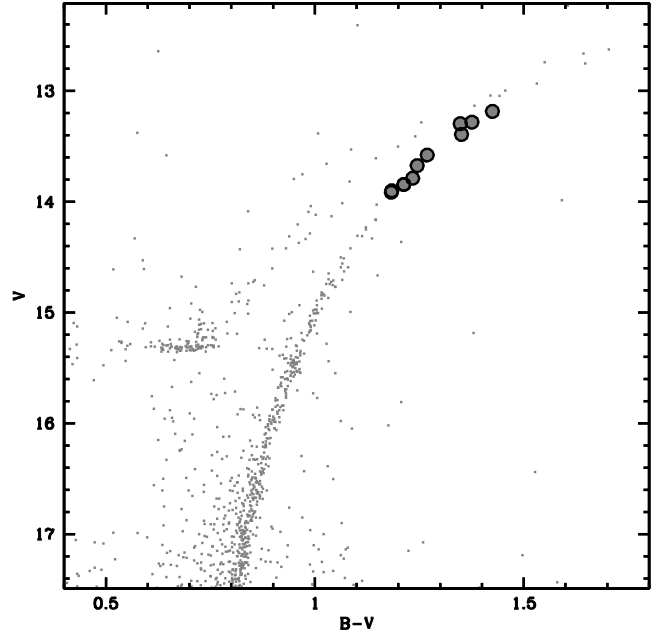


**Figure 1.** Optical ($v$, $B − v$) CMD of NGC 6362 in the innermost 300 arcsec (the photometry comes from the catalogue described in Dalessandro et al. 2014). The UVES targets are highlighted with black filled circles.

European Southern Observatory (ESO) Very Large Telescope. We used the combined MultiSpectroscopy mode+Ultraviolet and Visual Echelle Spectrograph (MEDUSA+UVES) configuration, which allowed the simultaneous allocation of eight UVES high-resolution fibres and 132 MEDUSA mid-resolution fibres per exposure. While the stars observed in the MEDUSA mode have been discussed in Mucciarelli et al. (2016), in this work we focus on the 11 stars observed with the UVES 580 Red Arm spectral configuration, with a resolution of $R \sim 45\,000$ in the spectral range ∼4800–6800 Å. Targets have been selected from the Wide Field Imager (WFI) photometric catalogue presented in Dalessandro et al. (2014). For this study, only red giant branch (RGB) stars brighter than $v < 14$ mag have been targeted (see Fig. 1 ). Also, to avoid contamination from neighbours, only stars with no close (i.e. within 2 arcsec) sources brighter than $v < v_{\rm target} + 1$ have been selected. Four exposures of 45 min for each target have been secured. Two UVES fibres have been used to sample the sky background, thus allowing a proper sky subtraction for each individual exposure.

To reduce the acquired data, we used the last version of the FLAMES-UVES Common Pipeline Libraries based ESO pipeline,[1] which includes bias-subtraction, flat-field correction, wavelength calibration with a standard Th-Ar lamp, extraction of one-dimensional spectra and order merging. The accuracy of the dispersion solution has been checked by comparing the observed position of several sky emission lines with their rest-frame position as reported in the sky lines atlas by Osterbrock et al. (1996). No significant wavelength shifts have been found. Once extracted, all the individual (sky-subtracted) exposures of each target have been brought to the same reference by correcting for the corresponding heliocentric radial velocity (see Section 2.1 for the details), and finally combined together to obtain a median spectrum. The final reduced spectra have a signal-to-noise ratio (SNR) larger than ∼30 at any wavelength.

---

[1] http://www.eso.org/sci/software/pipelines/

**Table 2.** NGC 6362 UVES targets analysed in this work.

| ID | RA (°) | Dec. (°) | $B$ (mag) | $v$ (mag) | $T_{eff}$ (K) | $\log g$ | $v_{turb}$ ( km s$^{-1}$) | $v_{rad}$ ( km s$^{-1}$) | $\sigma_{vrad}$ (km s$^{-1}$) |
|---|---|---|---|---|---|---|---|---|---|
| 601063 | 262.875 1296 | −67.097 0861 | 15.023 | 13.789 | 4308 | 1.33 | 1.5 | −14.39 | 0.06 |
| 602339 | 262.846 2133 | −67.010 0153 | 14.919 | 13.674 | 4292 | 1.27 | 1.5 | −14.23 | 0.12 |
| 709358 | 263.009 1350 | −67.056 4120 | 14.744 | 13.393 | 4147 | 1.05 | 1.5 | −15.24 | 0.07 |
| 710376 | 262.996 4883 | −67.042 5252 | 15.099 | 13.916 | 4382 | 1.43 | 1.4 | −17.39 | 0.13 |
| 711565 | 262.982 5550 | −67.037 3852 | 15.058 | 13.845 | 4338 | 1.37 | 1.5 | −10.75 | 0.07 |
| 716150 | 262.926 5237 | −67.060 8503 | 15.086 | 13.902 | 4381 | 1.42 | 1.5 | −16.01 | 0.06 |
| 601269 | 262.870 6968 | −67.104 1887 | 14.706 | 13.355 | 4147 | 1.04 | 1.6 | −13.42 | 0.09 |
| 604027 | 262.788 5538 | −67.115 7141 | 14.848 | 13.579 | 4259 | 1.21 | 1.5 | −14.98 | 0.08 |
| 703323 | 263.107 7119 | −67.044 2269 | 14.658 | 13.282 | 4114 | 0.98 | 1.5 | −17.33 | 0.09 |
| 714494 | 262.948 0400 | −67.037 2456 | 14.644 | 13.296 | 4151 | 1.02 | 1.5 | −14.02 | 0.07 |
| 716237 | 262.925 3519 | −67.038 1319 | 14.610 | 13.185 | 4051 | 0.90 | 1.5 | −17.93 | 0.11 |

*Notes.* Identification number, coordinates, $B$ and $v$ magnitudes, atmospheric parameters, heliocentric radial velocities and their uncertainties for the 11 UVES targets of NGC 6362 analysed in this work. The photometric parameters have been taken from the catalogue of Dalessandro et al. (2014).

## 2.1 Radial velocities

Radial velocities ($v_{rad}$) have been measured using the wrapper 4DAO[2] (Mucciarelli 2013), which allows to run DAOSPEC (Stetson & Pancino 2008) for large sets of spectra, tuning automatically its main input parameters. For all the 11 targets, we treated the two UVES chips of each single exposure independently. For the lower (L) chip, $v_{rad}$ have been computed by using ∼160 absorption lines, while for the upper (U) chip, the lines used were ∼190. For each target, we obtained a remarkably good agreement between the measurements of the two independent chips, finding an average difference of only $v_{rad, U} - v_{rad, L} = +0.06$ km s$^{-1}$ ($\sigma = 0.18$ km s$^{-1}$). Moreover, we did not find any significant difference among the $v_{rad}$ measured for the four exposures of each target. This indicates that none of the observed targets are binary systems. We then computed the final values of $v_{rad}$ as the average value of the eight single exposure measurements (two chips for each of the four exposures) and we adopted the dispersion around the mean divided by $\sqrt(8)$ as uncertainty. Heliocentric velocities and related errors are listed in Table 2.

We measured an average $v_{rad}$ of $v_{rad} = -15.03$ km s$^{-1}$ ($\sigma = 2.07$ km s$^{-1}$), which is in agreement with the value derived by Mucciarelli et al. (2016) ($v_{rad} = -13.8$ km s$^{-1}$, $\sigma = 2.7$ km s$^{-1}$). According to their $v_{rad}$ distribution, all the targeted stars are members having $v_{rad}$ values that lie well within $2\sigma$ from the systemic velocity.

## 3 CHEMICAL ANALYSIS

### 3.1 Atmospheric parameters

Effective temperatures ($T_{eff}$) and surface gravities ($\log g$) for target stars have been derived from their $B$ and $v$ magnitudes, in the same way as described in in Mucciarelli et al. (2016). We correct magnitudes and colours for differential reddening using the procedure outlined in Massari et al. (2012) (see also Milone et al. 2012). Differential reddening corrections across the whole WFI field of view range from $\delta[E(B − v)] = -0.03$ to $+0.03$ mag around the adopted average colour excess $E(B − v) = 0.09$ mag (Reed, Hesser & Shawl 1988).

Errors on the parameters affecting the determination of the absolute colour for the analysed targets, i.e. photometric errors or

[2] 4DAO is freely distributed at the website http://www.cosmiclab.eu/4dao/4dao.php.

uncertainty on the absolute and differential reddening ($\sigma_{[E(B − v)]}$ and $\sigma_{\delta[E(B−V)]}$, respectively) could potentially affect our $T_{eff}$ estimates. Thus, to evaluate the uncertainties on $T_{eff}$, we re-determined temperatures assuming typical errors on colours and extinction of $\sigma_{B, v} = 0.01$, $\sigma_{[E(B − v)]} = 0.04$ and $\sigma_{\delta[E(B − v)]} = 0.02$ mag, respectively. We underline that the quoted values are conservative upper limits, since the nominal photometric errors of such bright and well-exposed stars are <0.01 mag, while the errors on the absolute and differential reddening estimates correspond to about the 50 per cent of their value (see Dalessandro et al. 2014). Finally, we measure a typical uncertainty on $T_{eff}$ of ∼90 K.

Stars located in the brightest portion of the RGB, especially those approaching the RGB tip, can be significantly be affected by non-local thermodynamic equilibrium effects that spuriously decrease the iron abundances from Fe I lines leaving those from Fe II lines unaltered (see Ivans et al. 2001; Lapenna et al. 2014; Mucciarelli et al. 2015). This causes the spectroscopic derivation of $\log g$ through ionization equilibrium (i.e. $\log g$ is constrained by imposing that both neutral and ionized iron lines give the same abundance) to be systematically biased towards lower gravities. Thus, we prefer to rely on photometric gravities, derived by using the Stefan-Boltzmann relation. We adopted an absolute distance modulus of $(m − M)_0 = 14.4$ mag (from Harris 1996), bolometric corrections from Alonso, Arribas & Martínez-Roger (1999) and a mass of $0.75$ M$_\odot$. Such a mass has been derived from the best-fitting isochrone taken from the BaSTI data set (Pietrinferni et al. 2006), with an age of 12 Gyr, $Z = 0.004$ and $\alpha$-enhanced chemical mixture (corresponding to [Fe/H] = −1.01 dex). Uncertainties in $\log g$ have been computed by taking into account the errors on $T_{eff}$ (as described above), bolometric luminosity (due to all the photometric uncertainties) and mass (we assumed $\pm 0.05$ M$_\odot$, which corresponds to the range of masses that populate the entire RGB according to the best-fitting isochrone). The final uncertainty on $\log g$ is about 0.05 dex.

Finally, microturbulent velocities $v_{turb}$ have been derived spectroscopically, by requiring no trend between the measured iron abundances and the line strengths. Typical uncertainties on this parameter are about 0.1 km s$^{-1}$. The atmospheric parameters for each analysed target are shown in Table 2.

### 3.2 Abundance measurements

The adopted linelist has been compiled by selecting only transitions that are unblended at the temperatures, gravities and metallicities

**Table 3.** Elemental abundances for the analysed targets: [Fe/H], light-elements and $\alpha$-elements.

| ID | [Fe/H] | [Mg/Fe] | [Al/Fe] | [Si/Fe] | [Ca/Fe] | [Ti/Fe] |
|---|---|---|---|---|---|---|
| 601063 | $-1.06 \pm 0.05$ | $0.53 \pm 0.05$ | $0.46 \pm 0.06$ | $0.45 \pm 0.12$ | $0.29 \pm 0.08$ | $0.24 \pm 0.14$ |
| 602339 | $-1.08 \pm 0.05$ | $0.54 \pm 0.06$ | $0.49 \pm 0.06$ | $0.43 \pm 0.13$ | $0.24 \pm 0.08$ | $0.25 \pm 0.14$ |
| 709358 | $-1.07 \pm 0.02$ | $0.54 \pm 0.04$ | $0.53 \pm 0.07$ | $0.46 \pm 0.10$ | $0.25 \pm 0.08$ | $0.28 \pm 0.14$ |
| 710376 | $-1.04 \pm 0.06$ | $0.49 \pm 0.08$ | $0.53 \pm 0.07$ | $0.42 \pm 0.13$ | $0.29 \pm 0.08$ | $0.24 \pm 0.13$ |
| 711565 | $-1.11 \pm 0.06$ | $0.60 \pm 0.09$ | $0.49 \pm 0.06$ | $0.49 \pm 0.14$ | $0.25 \pm 0.09$ | $0.24 \pm 0.13$ |
| 716150 | $-1.06 \pm 0.06$ | $0.54 \pm 0.08$ | $0.57 \pm 0.07$ | $0.41 \pm 0.13$ | $0.24 \pm 0.09$ | $0.23 \pm 0.13$ |
| 601269 | $-1.07 \pm 0.04$ | $0.57 \pm 0.04$ | $0.47 \pm 0.07$ | $0.43 \pm 0.13$ | $0.28 \pm 0.08$ | $0.26 \pm 0.13$ |
| 604027 | $-1.07 \pm 0.05$ | $0.52 \pm 0.05$ | $0.56 \pm 0.08$ | $0.46 \pm 0.12$ | $0.29 \pm 0.09$ | $0.22 \pm 0.14$ |
| 703323 | $-1.10 \pm 0.04$ | $0.52 \pm 0.04$ | $0.56 \pm 0.07$ | $0.49 \pm 0.14$ | $0.24 \pm 0.08$ | $0.21 \pm 0.13$ |
| 714494 | $-1.08 \pm 0.04$ | $0.53 \pm 0.05$ | $0.54 \pm 0.07$ | $0.45 \pm 0.12$ | $0.28 \pm 0.08$ | $0.26 \pm 0.14$ |
| 716237 | $-1.03 \pm 0.05$ | $0.53 \pm 0.04$ | $0.46 \pm 0.08$ | $0.42 \pm 0.15$ | $0.26 \pm 0.09$ | $0.23 \pm 0.12$ |

*Notes.* Identification number, elemental abundances and related uncertainties for the same 11 targets described in Table 2. This table continues in Tables 4 and 5 for other groups of elements.

of sampled stars. Atomic data are from the latest version of the Kurucz+–Castelli data base, improved for some specific cases with new and updated values.

For the elements in our linelist with single and unblended lines, we estimated the chemical abundances from the measured equivalent width (EW), by using the package GALA (Mucciarelli et al. 2013b).[3] We run GALA keeping $T_{\text{eff}}$ and log $g$ of the model fixed and allowing its metallicity to vary iteratively in order to match the iron abundance measured from EWs. All the model atmospheres have been computed by means of the ATLAS9 code (Castelli & Kurucz 2004), while EWs were measured by using DAOSPEC through the code 4DAO (see Section 2.1). EW uncertainties are estimated by DAOSEPC as the standard deviation of the local flux residuals (see Stetson & Pancino 2008). All the lines with EW errors larger than 10 per cent were excluded from the analysis. Solar reference abundances are taken from Grevesse & Sauval (1998).

Only for the lines with hyperfine structure and/or isotopic splitting (Cu, Ba, Nd, Eu, La), abundances have been obtained by individually comparing the observed spectral lines with a grid of synthetic spectra computed with SYNTHE (Sbordone 2004), by running a $\chi^2$-minimization algorithm (see the procedure described in Mucciarelli et al. 2012). In particular, synthetic spectra – computed by assuming for each star the appropriate atmospheric parameters derived as described in Section 3.1 – are convolved at the UVES resolution and finally re-sampled at the pixel size as the observed spectra.

### 3.3 Abundance uncertainties

The total uncertainties on abundance measurements has been derived by considering two main sources of error: the internal error associated with the measurement procedure and the errors arising from the uncertainties in the atmospheric parameters.

We defined as internal error the dispersion around the mean divided by the square root of the number of lines used to compute abundances. Abundances of elements measured via spectral synthesis method (namely Cu, La and Eu) come from the measurement of only one line. In this case, the corresponding internal error has then been computed by means of Monte Carlo simulations. Briefly, Poissonian noise is added to the best-fitting synthetic spectrum in order to reproduce the observed SNR and then the procedure to derive the

abundance is repeated. The dispersion of the abundances measured from 1000 Monte Carlo realizations has been adopted as the internal abundance uncertainty. Depending on the SNR around these lines (ranging from 30 to 60), the typical internal errors obtained in this way range from 0.03 up to 0.11 dex.

In order to quantify the error coming from the uncertainties on the atmospheric parameters, we repeated the chemical analysis by varying each parameter for the corresponding uncertainty (see Section 3.1).

The total uncertainty on the [X/H] abundances has been computed by summing in quadrature this contribution and the intrinsic error described above. As discussed by McWilliam et al. (1995), this kind of uncertainty, when related to abundance ratios as [X/Y] = [X/H]-[Y/H], partially cancels out because lines of the same ionization stage tend to react in a similar way to changes in the stellar parameters. Therefore, we followed their prescription to calculate our final [X/Fe] abundance uncertainties.

## 4 RESULTS

In this section, the results of the chemical analysis are described for each elemental group. In particular, elemental abundances as found for NGC 6362 (always shown as a red empty star in Figs 3–8) are directly compared to abundances taken from the literature for other GCs (values from Carretta et al. 2009 are shown as green filled circles,[4] while data from Mészáros et al. 2015 are plotted as blue filled circles, if not stated otherwise) and Galactic field stars (grey dots; data from Fulbright 2000; Gratton et al. 2003; Reddy et al. 2003; Reddy, Lambert & Allende Prieto 2006). All the measured values and the corresponding uncertainties are listed in Tables 3–5, while the average abundance ratios are listed in Table 6.

(i) Iron abundances: By using the Maximum Likelihood (ML) algorithm described in Mucciarelli et al. (2012), we found that the iron distribution for our spectroscopic sample is best described by a Gaussian function with mean $\langle$[Fe I/H]$\rangle = -1.07 \pm 0.01$ and a null dispersion of $\sigma_{\text{[Fe I/H]}} = 0.00 \pm 0.01$. The derived Fe abundance agrees well with the value provided by Mucciarelli et al. (2016), i.e. [Fe I/H] $= -1.09 \pm 0.01$ dex. A very similar value is obtained from the single ionized Fe II lines that provide an average abundance of $\langle$[Fe II/H]$\rangle = -1.06 \pm 0.01$, with null dispersion.

---

[3] GALA is freely distributed at the Cosmic-Lab project website, http://www.cosmic-lab.eu/gala/gala.php.

[4] Ti abundances for several GCs have been provided by Carretta, private communication.

**Table 4.** Elemental abundance for the analysed targets: iron-peak elements.

| ID | [Sc/Fe] | [V/Fe] | [Cr/Fe] | [Mn/Fe] | [Co/Fe] | [Ni/Fe] | [Cu/Fe] |
|---|---|---|---|---|---|---|---|
| 601063 | 0.14 ± 0.06 | 0.03 ± 0.15 | − 0.09 ± 0.14 | − 0.34 ± 0.09 | 0.13 ± 0.10 | 0.00 ± 0.06 | − 0.14 ± 0.13 |
| 602339 | 0.20 ± 0.05 | 0.07 ± 0.15 | − 0.05 ± 0.15 | − 0.32 ± 0.10 | 0.14 ± 0.06 | − 0.04 ± 0.07 | − 0.15 ± 0.13 |
| 709358 | 0.19 ± 0.03 | 0.11 ± 0.14 | − 0.03 ± 0.15 | − 0.32 ± 0.09 | 0.17 ± 0.05 | 0.00 ± 0.04 | − 0.21 ± 0.12 |
| 710376 | 0.16 ± 0.07 | 0.04 ± 0.15 | 0.00 ± 0.14 | − 0.40 ± 0.10 | 0.08 ± 0.08 | − 0.03 ± 0.08 | − 0.12 ± 0.13 |
| 711565 | 0.23 ± 0.07 | 0.01 ± 0.13 | − 0.03 ± 0.15 | − 0.34 ± 0.10 | 0.14 ± 0.10 | 0.01 ± 0.07 | − 0.21 ± 0.13 |
| 716150 | 0.15 ± 0.07 | 0.03 ± 0.14 | − 0.09 ± 0.15 | − 0.33 ± 0.10 | 0.10 ± 0.07 | − 0.05 ± 0.07 | − 0.18 ± 0.13 |
| 601269 | 0.21 ± 0.04 | 0.11 ± 0.13 | − 0.02 ± 0.14 | − 0.29 ± 0.09 | 0.13 ± 0.05 | − 0.02 ± 0.06 | − 0.20 ± 0.12 |
| 604027 | 0.17 ± 0.06 | 0.03 ± 0.14 | − 0.02 ± 0.15 | − 0.34 ± 0.10 | 0.09 ± 0.05 | − 0.03 ± 0.05 | − 0.13 ± 0.13 |
| 703323 | 0.20 ± 0.05 | 0.08 ± 0.13 | − 0.03 ± 0.13 | − 0.34 ± 0.10 | 0.13 ± 0.05 | − 0.03 ± 0.06 | − 0.19 ± 0.12 |
| 714494 | 0.18 ± 0.04 | 0.10 ± 0.13 | − 0.01 ± 0.14 | − 0.33 ± 0.10 | 0.12 ± 0.06 | − 0.04 ± 0.06 | − 0.16 ± 0.12 |
| 716237 | 0.12 ± 0.05 | 0.18 ± 0.15 | − 0.02 ± 0.15 | − 0.34 ± 0.09 | 0.15 ± 0.06 | − 0.03 ± 0.06 | − 0.29 ± 0.13 |

**Table 5.** Elemental abundance for the analysed targets: s-elements and r- elements.

| ID | [Ba/Fe] | [La/Fe] | [Nd/Fe] | [Eu/Fe] |
|---|---|---|---|---|
| 601063 | 0.63 ± 0.13 | 0.45 ± 0.07 | 0.26 ± 0.08 | 0.49 ± 0.06 |
| 602339 | 0.60 ± 0.11 | 0.35 ± 0.07 | 0.25 ± 0.07 | 0.37 ± 0.06 |
| 709358 | 0.64 ± 0.12 | 0.35 ± 0.04 | 0.22 ± 0.04 | 0.48 ± 0.04 |
| 710376 | 0.53 ± 0.13 | 0.29 ± 0.08 | 0.18 ± 0.08 | 0.32 ± 0.07 |
| 711565 | 0.67 ± 0.12 | 0.42 ± 0.09 | 0.36 ± 0.08 | 0.51 ± 0.07 |
| 716150 | 0.60 ± 0.12 | 0.38 ± 0.08 | 0.24 ± 0.09 | 0.38 ± 0.07 |
| 601269 | 0.66 ± 0.11 | 0.41 ± 0.07 | 0.29 ± 0.07 | 0.50 ± 0.06 |
| 604027 | 0.60 ± 0.13 | 0.35 ± 0.08 | 0.21 ± 0.08 | 0.43 ± 0.05 |
| 703323 | 0.63 ± 0.12 | 0.38 ± 0.08 | 0.24 ± 0.09 | 0.44 ± 0.07 |
| 714494 | 0.61 ± 0.11 | 0.37 ± 0.07 | 0.24 ± 0.08 | 0.43 ± 0.05 |
| 716237 | 0.54 ± 0.02 | 0.26 ± 0.08 | 0.15 ± 0.08 | 0.41 ± 0.06 |

**Table 6.** Comparison between NGC 6362 and M 4.

| Element | NGC 6362 | M 4 |
|---|---|---|
| ⟨[Fe/H]⟩ | − 1.07 ± 0.01 | − 1.14 ± 0.01 |
| ⟨[Mg/Fe]⟩ | 0.54 ± 0.01 | 0.50 ± 0.02 |
| ⟨[Al/Fe]⟩ | 0.51 ± 0.02 | 0.63 ± 0.02 |
| ⟨[Si/Fe]⟩ | 0.45 ± 0.03 | 0.50 ± 0.02 |
| ⟨[Ca/Fe]⟩ | 0.26 ± 0.02 | 0.26 ± 0.02 |
| ⟨[Sc/Fe]⟩ | 0.18 ± 0.02 | 0.23 ± 0.01 |
| ⟨[Ti/Fe]⟩ | 0.24 ± 0.04 | 0.19 ± 0.03 |
| ⟨[V/Fe]⟩ | 0.07 ± 0.04 | − 0.02 ± 0.03 |
| ⟨[Cr/Fe]⟩ | − 0.05 ± 0.04 | − 0.09 ± 0.03 |
| ⟨[Mn/Fe]⟩ | − 0.33 ± 0.02 | − 0.30 ± 0.04 |
| ⟨[Co/Fe]⟩ | 0.12 ± 0.02 | 0.10 ± 0.02 |
| ⟨[Ni/Fe]⟩ | − 0.02 ± 0.01 | 0.02 ± 0.02 |
| ⟨[Cu/Fe]⟩ | − 0.18 ± 0.03 | − 0.17 ± 0.03 |
| ⟨[Ba/Fe]⟩ | 0.61 ± 0.01 | 0.71 ± 0.04 |
| ⟨[La/Fe]⟩ | 0.36 ± 0.02 | 0.51 ± 0.02 |
| ⟨[Nd/Fe]⟩ | 0.37 ± 0.02 | 0.42 ± 0.02 |
| ⟨[Eu/Fe]⟩ | 0.43 ± 0.01 | 0.49 ± 0.01 |

*Note.* Average elemental abundances and related uncertainties as found for the two samples of giants in NGC 6362 and M 4.

(ii) Light elements: Mg, Al: As already demonstrated by Mucciarelli et al. (2016) for a larger sample of stars including the 11 targets studied here, NGC 6362 displays a broad [Na/Fe] distribution, with the presence of two (equally populated) stellar groups, peaked at [Na/Fe] = +0.00 and +0.33 dex. Another significant feature related to the existence of MPs in the form of light element abundance spreads is the presence of star-to-star variations in Mg and Al abundances. This feature arises as an anticorrelation in a few
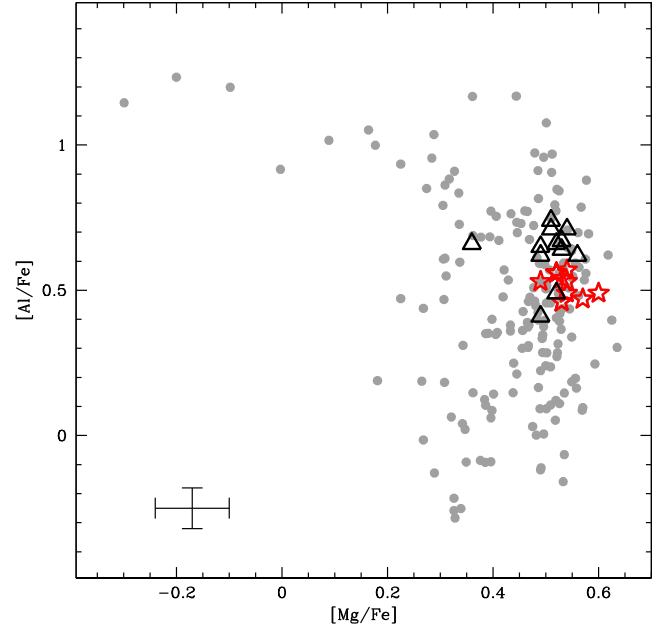


**Figure 2.** [Al/Fe] abundance ratio as a function of [Mg/Fe] for the 11 UVES targets of NGC 6362 analysed in this work (red stars), for 12 giants belonging to M 4 (black triangles), and for 17 Galactic GCs (grey dots, data from Carretta et al. 2009). Typical errors are shown in the bottom left-hand region of the plot.

clusters, whereas a large Al variation is coupled with a small or null Mg variation in most cases (Carretta et al. 2009).

As shown in Fig. 2, NGC 6362 does not display intrinsic variations in both Mg and Al. In fact, NGC 6362 stars describe only a clump with very small dispersion compared to the whole extent of the anticorrelation covered by the UVES targets analysed in Carretta et al. (2009) in 17 GCs (grey dots). According to an ML analysis, the mean abundances and intrinsic dispersions for these two elements are ⟨[Mg/Fe]⟩ = +0.54 ± 0.01, $\sigma_{\text{[Mg/Fe]}}$ = 0.00 ± 0.01 and ⟨[Al/Fe]⟩ = + 0.51 ± 0.02, $\sigma_{\text{[Al/Fe]}}$ = 0.00 ± 0.02, thus confirming the lack for any abundance spread in both [Mg/Fe] and [Al/Fe].

In Fig. 3, the average Mg and Al abundances of NGC 6362 stars are compared to those of Galactic field stars.[5] Although NGC 6362 stars appear to be quite rich in both Mg and Al content with respect

---

[5] We decided not to display other Galactic GCs in the plot, as for those showing intrinsic spread in Mg and Al abundance, an average value is not meaningful.
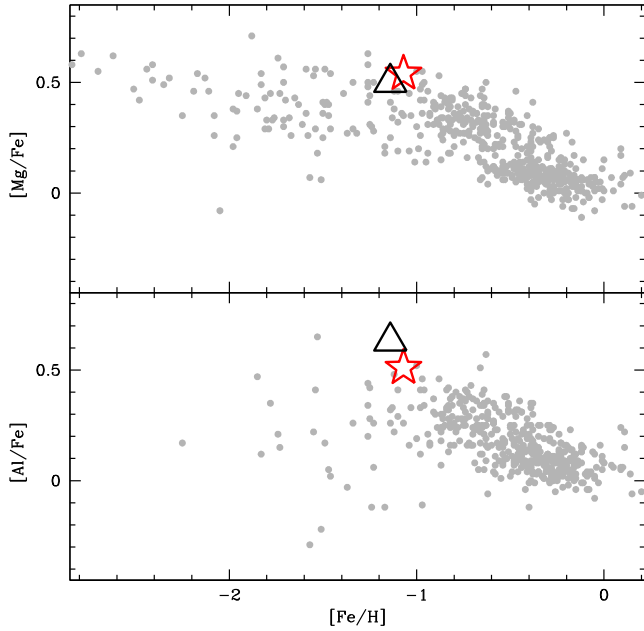
**Figure 3.** Upper panel: [Mg/Fe] versus [Fe/H] trends for NGC 6362 (red star) and M 4 (black triangle), compared to a sample of field stars (grey dots). Lower panel: same comparison for [Al/Fe].



**Figure 4.** Upper three panels: [Si/Fe], [Ca/Fe], [Ti/Fe] versus [Fe/H] trends for NGC 6362, field stars (same symbols of Fig. 3) and Galactic GCs (green circles are taken from Carretta et al. 2009, blue circles are taken from Mészáros et al. 2015). Lower panel: same comparison on the [α/Fe] versus [Fe/H] trend. NGC 6362 is in very good agreement with what observed for the other GCs.

to stars at similar same metallicity (upper and lower panel of Fig. 3, respectively), their Mg and Al abundances are still in agreement with the trends observed for field stars.

(iii) α-elements: Si, Ca and Ti: We adopt the α-elements produced by explosive nucleosynthesis (Si, Ca and Ti) as tracers of the total α-element abundance for the cluster. Mg (which is produced by hydrostatic nucleosynthesis) is excluded from this discussion because self-enrichment processes can, in principle, alter its initial abundance (even if in NGC 6362 no evidence of an Mg spread is found).

When analysed separately, Si is the element with the highest average enhancement, having $\langle[Si/Fe]\rangle = +0.45 \pm 0.03$, while Ca and Ti show lower values that are very similar each other, $\langle[Ca/Fe]\rangle = +0.26 \pm 0.02$ and $\langle[Ti/Fe]\rangle = +0.24 \pm 0.04$, respectively. According to the ML analysis, none of the three elements show any hints of intrinsic dispersion. Fig. 4 shows the comparison among NGC 6362, and the same objects as those shown in Fig. 3. Also in terms of Si, Ca and Ti content, NGC 6362 does not behave differently from what commonly is observed for the other populations.

(iv) Iron-peak elements: Sc, V, Mn, Cr, Co and Ni: We measured abundances for six iron-peak elements, namely Sc, V, Mn, Cr, Co and Ni.

For Cr and Ni, the abundances have been derived from the EW measurement, and both the abundances of these elements turn out to be scaled-solar, with average values of $\langle[Cr/Fe]\rangle = -0.05 \pm 0.04$ and $\langle[Ni/Fe]\rangle = -0.02 \pm 0.01$.

For odd-Z elements like Sc and Mn, we used the spectral synthesis method since their lines suffer for hyperfine splitting. In this case, we found a supersolar [Sc/Fe] abundance ratio, with an average $\langle[ScII/Fe]\rangle = +0.18 \pm 0.01$, while we found a significant deficiency in the Mn content of the cluster ($\langle[Mn/Fe]\rangle = -0.33 \pm 0.02$).

Finally, the presence of both isolated lines and lines split for hyperfine structure for V and Co within the UVES wavelength range allowed us to check for possible systematic effects arising from the different method of analysis used. For both the elements, we found that the abundances measured with the EW method and those
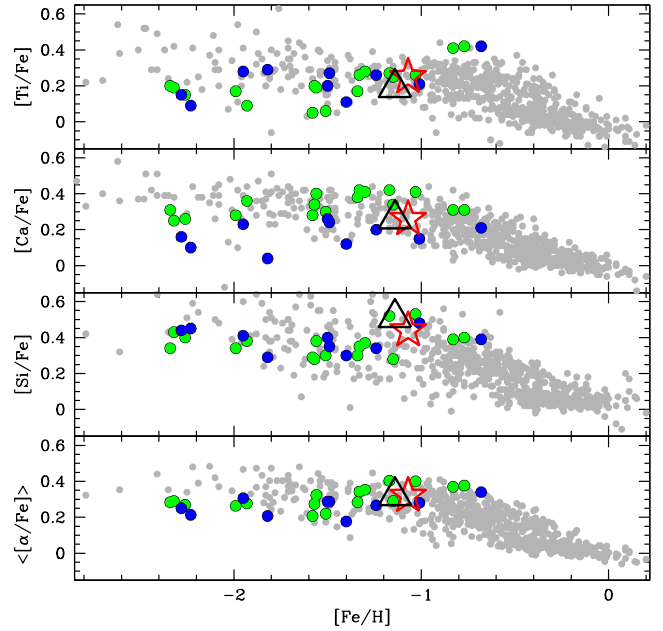
coming from the spectral synthesis agree very well, being coincident within a 1σ uncertainty. In particular, we obtained slightly supersolar abundance ratios for both V ($\langle[V/Fe]_{EW}\rangle = +0.07 \pm 0.04$ and $\langle[V/Fe]_{synthesis}\rangle = +0.10 \pm 0.05$, respectively) and Co ($\langle[Co/Fe]_{EW}\rangle = +0.12 \pm 0.02$ and $\langle[Co/Fe]_{synthesis}\rangle = +0.09 \pm 0.02$). Therefore, we can safely claim that no systematic uncertainties are introduced by the use of two different abundance measurement methods.

The iron-peak elemental abundances for NGC 6362 are compared to the typical values found for field stars in Fig. 5.

(v) Copper, s-elements and r- elements: The abundances for these elements have all been measured by means of spectral synthesis.

For Cu, the only available transition is that at 5105 Å, since the other Cu optical line (at 5782 Å) falls in the gap between the two UVES chips. NGC 6362 behaves similarly to the other (few) GCs in the Galaxy for which Cu measurements exist (see Cunha et al. 2002; Simmerer et al. 2003), with an average $\langle[Cu/Fe]\rangle = -0.18 \pm 0.03$. This is also in good agreement with measurements for field stars at similar [Fe/H] (see the upper panel of Fig. 6).

We determined the abundance of the slow neutron-capture elements Ba, Nd and La. Regarding the abundance of Ba, we measured $\langle[BaII/Fe]\rangle = +0.56 \pm 0.01$. By using only the La line at 6390.5 Å (Lawler, Bonvallet & Sneden 2001), we derived $\langle[LaII/Fe]\rangle = +0.36 \pm 0.02$, while for Nd, we found $\langle[Nd/Fe]\rangle = +0.37 \pm 0.02$.

Finally, we estimated the abundance of the rapid neutron-capture element Eu by using the transition at 6645.1 Å, finding $\langle[Eu/Fe]\rangle = +0.43 \pm 0.01$. NGC 6362 matches well the typical behaviour of [Eu/Fe] measured for the other GCs in the Galaxy (see the bottom panel of Fig. 6, where data for Eu abundances in 14 GCs have been taken from Sneden et al. 1997, 2004; Ivans, Sneden & Kraft 1999; Ivans et al. 2001; Lee & Carney 2002; Ramírez &
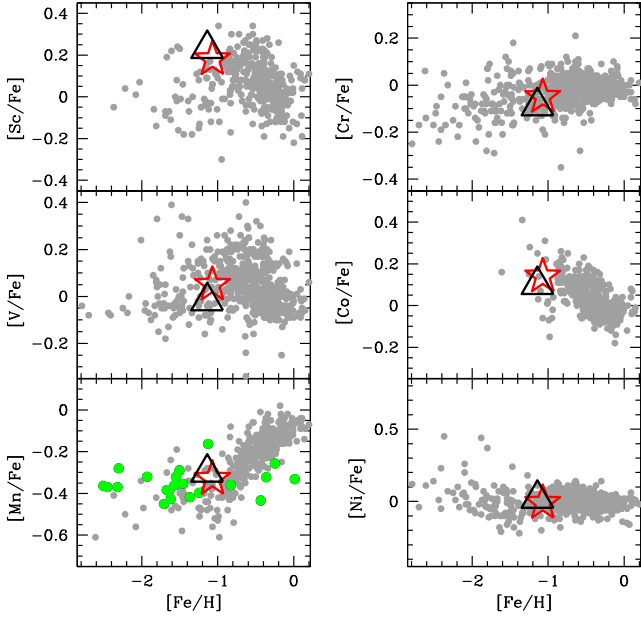
**Figure 5.** Comparison among the trends of the iron-peak element abundances versus [Fe/H] as measured for NGC 6362, M 4 and field stars. Green circles indicate the [Mn/Fe] average abundances derived by (Sobeck et al. 2006) for 21 Galactic GCs.
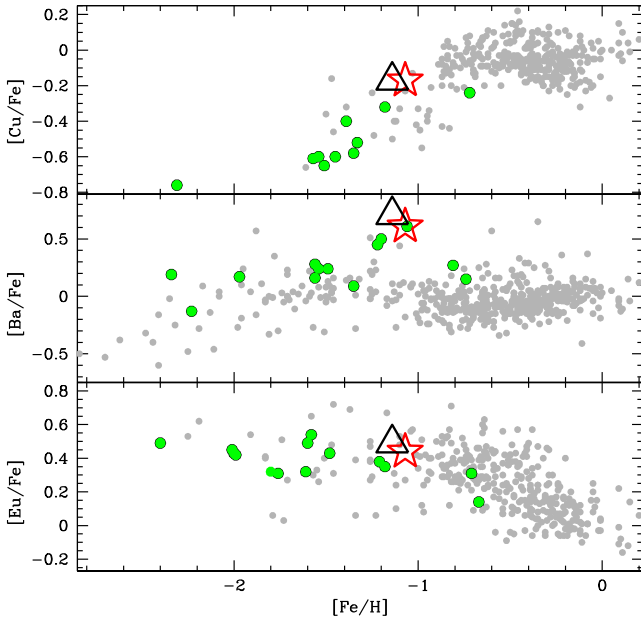


**Figure 7.** Comparison among the elemental abundances measured for NGC 6362 (red stars) and M 4 (black triangles).



**Figure 6.** Upper panel: [Cu/Fe] versus [Fe/H] trends for a sample of Galactic GCs (green circles) taken from (Simmerer et al. 2003), a sample of thick disc stars taken from (Reddy et al. 2003, 2006) and the cluster under analysis. Central panel: observed Ba trends for the same populations (data for the 14 plotted GCs have been taken from D'Orazi et al. 2010). Lower panel: same comparison but for Eu abundances.

Cohen 2002; Carretta et al. 2004; James et al. 2004; Yong et al. 2005; Carretta 2006; Marino et al. 2015).

### 4.1 Analysis of M 4 as a reference

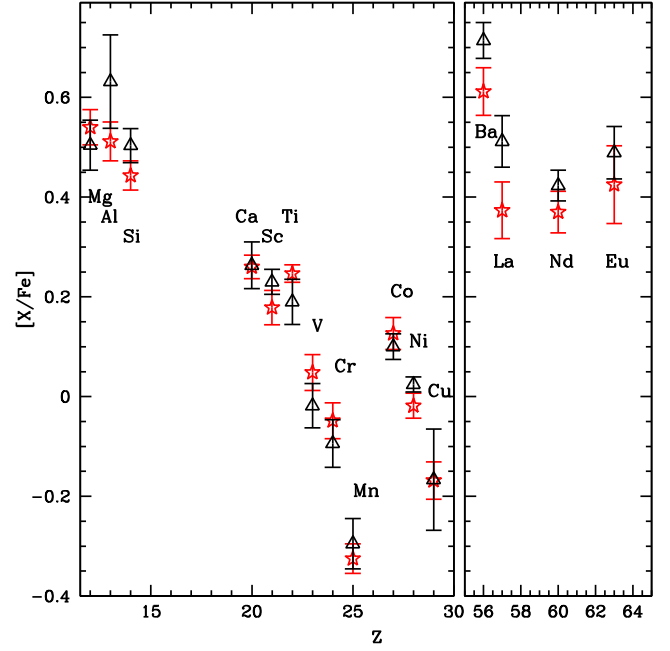In the previous paragraphs, we compared the elemental abundances of NGC 6362 with those of field stars and other GCs available in the literature. However, such a comparison could be prone to systematic effects due to, for example, different used instruments or adopted linelists, atomic parameters, model atmospheres, etc. To provide a further comparison free from all of these systematics, we decided to repeat our analysis on another GC with mass (see McLaughlin & van der Marel 2005) and metallicity very similar to those of NGC 6362: M 4. This differential comparison between two clusters with similar properties and analysed with the same procedure will allow us to accurately highlight any intrinsic difference among their chemical composition. Following the same approach described by Mucciarelli et al. (2013a), we thus re-analysed 12 RGB stars belonging to M 4 and observed with FLAMES-UVES Red Arm 580 (ID 073.0211, PI:Carretta). $B$ and $v$ magnitudes for M 4 have been obtained from the analysis of a data set of WFI 2.2-m images (programme 68.D-0265(A), PI: Ortolani), and have been corrected for differential reddening. The distance modulus $((m − M)_0 = 11.78$ mag) and colour excess $(E(B − v) = 0.32)$ mag have been taken from Bedin et al. (2009). Atmospheric parameters for the M4 targets have been obtained following the same approach used for the NGC 6362 stars. The results of such an investigation are shown in Figs 3–8, where abundance ratios for M 4 are always shown as black triangles. The average values are listed in Table 6, where the one-to-one comparison between the NGC 6362 and M 4 is displayed.

As a first step, we checked that the abundance ratios we obtained as output of our analysis were in agreement with previous results available in the literature. The iron abundance we measured for M 4 is ⟨[Fe/H]⟩ = −1.14 ± 0.01. This value is in good agreement with previous metallicity determinations obtained from giant stars (see Carretta et al. 2009; Mucciarelli et al. 2011; Villanova & Geisler 2011; Monaco et al. 2012. Mg and Al abundance ratios are shown in Fig. 2 as black triangles. Like NGC 6362 stars, they describe a compact clump as well, with no dispersion in Mg and only a small hint of dispersion in Al, confirmed by the ML analysis that found $\sigma_{[Al/Fe]} = 0.05 ± 0.03$ (a small Al dispersion for the cluster has also been found by Marino et al. 2008). Their
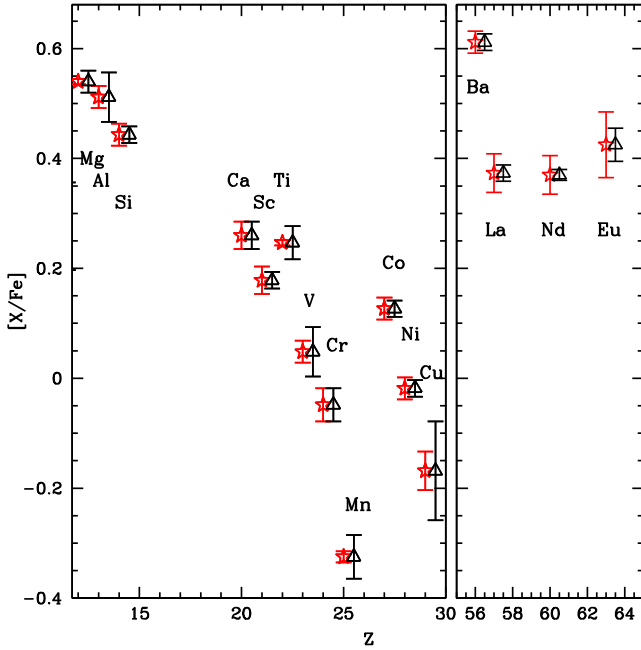
**Figure 8.** Comparison among the elemental IQR for NGC 6362 (red bars) and M 4 (black bars). For the sake of comparison, all the pars are plotted at the same *y*-axis value (that measured for NGC 6362).

average values are shown in Fig. 3, and agree well with the results in Marino et al. (2008) and Ivans et al. (1999), as α-peak and iron-peak elemental abundances do. It is worth noticing that for M 4, Simmerer et al. (2003) found $\langle[Cu/Fe]\rangle = -0.32$ dex by using both the Cu lines previously described. These authors used the same solar values and oscillator strength for the line used by us, and they obtained agreement within 0.1 dex between measurements coming from the two lines individually. Therefore, their estimate is compatible with ours to within ∼1σ. Finally, our measurement of $\langle[Ba/Fe]\rangle = +0.71 \pm 0.04$ for M 4 is ∼0.3 dex larger than that found in Marino et al. (2008). However, these authors used a solar value $A(Ba)_\odot = 2.45$ instead of our $A(Ba)_\odot = 2.13$. Therefore, such a discrepancy cancels out when the different adopted solar values are taken into account.

At this point, we performed the direct, one-to-one comparison between the chemistry of the two clusters, shown in Fig. 7. In general, we found that the agreement between the elemental abundances of NGC 6362 and M 4 is remarkable. In fact, all the elemental abundance ratio match within a 1σ uncertainty, with the only exception of [Ba II/Fe] and [La II/Fe], for which the agreement is only within a 2σ uncertainty.

## 5 DISCUSSION AND CONCLUSIONS

We measured abundance ratios for different elemental groups in the Galactic GC NGC 6362, which has never been investigated before using high-resolution spectroscopy, and we compared it with other GCs in the Milky Way.

With the aim of anchoring our findings to a solid touchstone, we also repeated the same chemical analysis (thus erasing any systematics) on a sample of RGB stars in M 4, a cluster that shares with NGC 6362 very similar mass and metallicity. Figs 7 and 8 show the comparison of the measured abundance ratios in NGC 6362 (red stars) and M 4 (black triangles), using the average values and the interquartile-range (IQR), respectively.

(i) Light elements: Mucciarelli et al. (2016) demonstrated that NGC 6362 hosts two distinct populations with different Na abundances. While Na star-to-star variations have been observed in most GCs, Mg and Al intrinsic spreads are not universal. In particular, according to both observations (see e.g. Carretta et al. 2009) and theoretical predictions (Ventura et al. 2014), the Al production in GCs depends on two main parameters: (i) metallicity, since a high metallicity causes lower Al-yields from polluters[6] (Ventura & D'Antona 2009; Karakas 2010; O'Connell et al. 2011), and (*ii*) cluster mass, since (under the hypothesis of the same initial mass function) a more massive cluster would have more polluters and would retain more polluted gas within its potential well. However, several exceptions to these trends exist, such as 47 Tucanae (which shows a small Al spread despite being quite massive; see Cordero et al. 2014) or M71 (which is an outlier in the Carretta relation; see Carretta et al. 2009; Cordero et al. 2015). Therefore, the Al abundances measured in this work for NGC 6362 and their comparison to M 4 are of particular interest.

As already shown is Section 4, Mg and Al internal variations in NGC 6362 are compatible with being null (see also Fig. 8), while M 4 stars show a possible small dispersion in Al content. The corresponding IQRs are extremely small as well, being of a few hundredths of dex for Mg and only slightly larger for Al ($IQR_{Al}^{NGC6362} = 0.04$ dex, $IQR_{Al}^{M4} = 0.09$ dex). Therefore, we can conclude that in terms of light element abundance, NGC 6362 behaves as the other GCs with similar mass and metallicity, both according to the differential analysis with respect to M 4 and observational-based prediction of Carretta et al. (2009).

(ii) α-peak and iron-peak elements: NGC 6362 is characterized by enhanced abundances for all the measured α-elements, with an average value of $\langle[\alpha/Fe]\rangle = +0.32$. This value matches well those measured in M 4 and in the other Galactic GCs (see e.g. Pritzl et al. 2005; Carretta et al. 2010; Mészáros et al. 2015). This finding confirms that NGC 6362 formed from gas enriched by core-collapse supernovae in a similar way to other Galactic GCs (excluding some GCs likely accreted by extragalactic galaxies and characterized by lower [α/Fe] ratios). In particular, NGC 6362 and M 4 show very similar α abundances, suggesting that they share a similar chemical enrichment by core-collapse supernovae. Also for the iron-peak elements, the analysis shows that NGC 6362 follows the same abundance patterns of the other GCs and no remarkable (element-by-element) difference is found between NGC 6362 and M 4.

(iii) s-process and r-process elements: The cluster has a [Ba/Fe] abundance ratio compatible with those of GCs of similar metallicity, like M4, NGC 288 and NGC 6171, and, in general, agrees well with the run of [s/Fe] abundance ratios with [Fe/H] (see fig. 1 in D'Orazi et al. 2010). In fact, metal-poor GCs show roughly solar [Ba/Fe] ratios, as the production of Ba at those metallicities is dominated by r-processes. On the other hand, [Ba/Eu] increases with increasing metallicity, because of the higher efficiency of the s-process. In the case of NGC 6362, [Ba/Eu] reaches 0.18 dex, compatible with the value measured in M 4 ([Ba/Eu] = 0.22 dex) and the same is observed also for [La/Eu] and [Nd/Eu]. Even if NGC 6362 has a [Ba/Fe] compatible with that of M 4 at a level of 2σ (at variance with the other abundance ratios that are compatible within 1σ), the two clusters show the same relative efficiency of s-process to r-process. Therefore, the general enhancement of s-process element

---

[6] This is true for AGB polluters, while no detailed Al-yields predictions are currently available for fast massive rotating stars (Decressin et al. 2007) or supermassive stars (Denissenkov & Hartwick 2014).

abundances measured in NGC 6362 suggests that the first generation of cluster stars (i) formed from gas already enriched by low-mass ($\sim$1–4 M$_\odot$) AGB stars, which are the main producers of s-process elements, the so-called main-component (see e.g. Busso, Gallino & Wasserburg 1999; Travaglio et al. 2004), and (ii) did not introduce any spread in the s-process abundance of second-generation stars.

Summing up, the differential comparison between NGC 6362 and M 4 revealed that all the elemental abundances measured for the two clusters match within 1$\sigma$ (with the marginal exception of [Ba/Fe]). None of the elements analysed in this work show any internal spread in NGC 6362. It is worth noting that NGC 6362 and M 4 also display the same extent of Na variation (see Mucciarelli et al. 2016).

According to the compilation of GC masses in McLaughlin & van der Marel (2005), and of GC metallicities in Harris (1996), the only clusters with properties similar to NGC 6362 and M 4 (and not associated with the Sagittarius dwarf spheroidal galaxy; see Law & Majewski 2010) that have been chemically investigated in detail are NGC 288 and NGC 6171. They both belong to the sample of clusters studied by Carretta et al. (2009), and as such they are plotted in Fig. 4, in the same metallicity range as that of NGC6362. Their chemical composition is consistent with that of the two clusters analysed in this work. Therefore, we conclude that NGC 6362 is a regular GC that shows the chemical composition representative of the Milky Way GCs with similar mass and metallicity, with the signatures of chemical enrichment by core-collapse supernovae and AGB stars.

## ACKNOWLEDGEMENTS

## REFERENCES

Alonso A., Arribas S., Martínez-Roger C., 1999, A&AS, 140, 261
Bastian N., Lamers H. J. G. L. M., de Mink S. E., Longmore S. N., Goodwin S. P., Gieles M., 2013, MNRAS, 436, 2398
Bedin L. R., Salaris M., Piotto G., Anderson J., King I. R., Cassisi S., 2009, ApJ, 697, 965
Busso M., Gallino R., Wasserburg G. J., 1999, ARA&A, 37, 239
Carretta E., 2006, AJ, 131, 1766
Carretta E., Gratton R. G., Bragaglia A., Bonifacio P., Pasquini L., 2004, A&A, 416, 925
Carretta E. et al., 2009, A&A, 505, 117
Carretta E., Bragaglia A., Gratton R., Lucatello S., Bellazzini M., D'Orazi V., 2010, ApJ, 712, L21
Carretta E., Bragaglia A., Gratton R. G., D'Orazi V., Lucatello S., Sollima A., 2014, A&A, 561, A87
Castelli F., Kurucz R. L., 2004, preprint (astro-ph/0405087)
Cordero M. J., Pilachowski C. A., Johnson C. I., McDonald I., Zijlstra A. A., Simmerer J., 2014, ApJ, 780, 94
Cordero M. J., Pilachowski C. A., Johnson C. I., Vesperini E., 2015, ApJ, 800, 3
Cunha K., Smith V. V., Suntzeff N. B., Norris J. E., Da Costa G. S., Plez B., 2002, AJ, 124, 379
D'Ercole A., Vesperini E., D'Antona F., McMillan S. L. W., Recchi S., 2008, MNRAS, 391, 825
D'Orazi V., Gratton R., Lucatello S., Carretta E., Bragaglia A., Marino A. F., 2010, ApJ, 719, L213
Dalessandro E. et al., 2014, ApJ, 791, L4
Dalessandro E., Lapenna E., Mucciarelli A., Origlia L., Ferraro F. R., Lanzoni B., 2016, ApJ, 829, 77
de Mink S. E., Pols O. R., Langer N., Izzard R. G., 2009, A&A, 507, L1
Decressin T., Meynet G., Charbonnel C., Prantzos N., Ekström S., 2007, A&A, 464, 1029
Denissenkov P. A., Hartwick F. D. A., 2014, MNRAS, 437, L21
Fulbright J. P., 2000, AJ, 120, 1841
Goldsbury R., Richer H. B., Anderson J., Dotter A., Sarajedini A., Woodley K., 2010, AJ, 140, 1830
Gratton R. G., Carretta E., Desidera S., Lucatello S., Mazzei P., Barbieri M., 2003, A&A, 406, 131
Gratton R., Sneden C., Carretta E., 2004, ARA&A, 42, 385
Gratton R. G., Carretta E., Bragaglia A., 2012, A&AR, 20, 50
Grevesse N., Sauval A. J., 1998, Space Sci. Rev., 85, 161
Harris W. E., 1996, AJ, 112, 1487
Ivans I. I., Sneden C., Kraft R. P., 1999, Ap&SS, 265, 195
Ivans I. I., Kraft R. P., Sneden C., Smith G. H., Rich R. M., Shetrone M., 2001, AJ, 122, 1438
James G., François P., Bonifacio P., Carretta E., Gratton R. G., Spite F., 2004, A&A, 427, 825
Karakas A. I., 2010, MNRAS, 403, 1413
Lapenna E., Mucciarelli A., Lanzoni B., Ferraro F. R., Dalessandro E., Origlia L., Massari D., 2014, ApJ, 797, 124
Law D. R., Majewski S. R., 2010, ApJ, 718, 1128
Lawler J. E., Bonvallet G., Sneden C., 2001, ApJ, 556, 452
Lee J.-W., Carney B. W., 2002, AJ, 124, 1511
McLaughlin D. E., van der Marel R. P., 2005, ApJS, 161, 304
McWilliam A., Preston G. W., Sneden C., Searle L., 1995, AJ, 109, 2757
Marino A. F., Villanova S., Piotto G., Milone A. P., Momany Y., Bedin L. R., Medling A. M., 2008, A&A, 490, 625
Marino A. F. et al., 2015, MNRAS, 450, 815
Massari D. et al., 2012, ApJ, 755, L32
Mészáros S. et al., 2015, AJ, 149, 153
Milone A. P. et al., 2012, ApJ, 744, 58
Monaco L., Villanova S., Bonifacio P., Caffau E., Geisler D., Marconi G., Momany Y., Ludwig H.-G., 2012, A&A, 539, A157
Mucciarelli A., 2013, preprint (arXiv:1311.1403)
Mucciarelli A., Origlia L., Ferraro F. R., Pancino E., 2009, ApJ, 695, L134
Mucciarelli A., Salaris M., Lovisi L., Ferraro F. R., Lanzoni B., Lucatello S., Gratton R. G., 2011, MNRAS, 412, 81
Mucciarelli A., Bellazzini M., Ibata R., Merle T., Chapman S. C., Dalessandro E., Sollima A., 2012, MNRAS, 426, 2889
Mucciarelli A., Bellazzini M., Catelan M., Dalessandro E., Amigo P., Correnti M., Cortés C., D'Orazi V., 2013a, MNRAS, 435, 3667
Mucciarelli A., Pancino E., Lovisi L., Ferraro F. R., Lapenna E., 2013b, ApJ, 766, 78
Mucciarelli A., Lapenna E., Massari D., Ferraro F. R., Lanzoni B., 2015, ApJ, 801, 69
Mucciarelli A. et al., 2016, ApJ, 824, 73
Muñoz C., Geisler D., Villanova S., 2013, MNRAS, 433, 2006
O'Connell J. E., Johnson C. I., Pilachowski C. A., Burks G., 2011, PASP, 123, 1139
Osterbrock D. E., Fulbright J. P., Martel A. R., Keane M. J., Trager S. C., Basri G., 1996, PASP, 108, 277
Pasquini L. et al., 2002, The Messenger, 110, 1
Paust N. E. Q. et al., 2010, AJ, 139, 476
Pietrinferni A., Cassisi S., Salaris M., Castelli F., 2006, ApJ, 642, 797
Piotto G., 2009, in Mamajek E. E., Soderblom D. R., Wyse R. F. G., eds, Proc. IAU Symp. 258, The Ages of Stars. Kluwer, Dordrecht, p. 233
Piotto G. et al., 2015, AJ, 149, 91

Pritzl B. J., Venn K. A., Irwin M., 2005, AJ, 130, 2140

Ramírez S. V., Cohen J. G., 2002, AJ, 123, 3277

Reddy B. E., Tomkin J., Lambert D. L., Allende Prieto C., 2003, MNRAS, 340, 304

Reddy B. E., Lambert D. L., Allende Prieto C., 2006, MNRAS, 367, 1329

Reed B. C., Hesser J. E., Shawl S. J., 1988, PASP, 100, 545

Renzini A., Buzzoni A., 1986, in Contopoulos I., Gabuzda D., Kylafis N., eds, Astrophysics and Space Science Library, Vol. 122, Spectral Evolution of Galaxies. Reidel Publ. Co., Dordrecht, p. 195

Renzini A. et al., 2015, MNRAS, 454, 4197

Sbordone L., 2004, PhD thesis, Universita degli studi di Roma

Simmerer J., Sneden C., Ivans I. I., Kraft R. P., Shetrone M. D., Smith V. V., 2003, AJ, 125, 2018

Sneden C., Kraft R. P., Shetrone M. D., Smith G. H., Langer G. E., Prosser C. F., 1997, AJ, 114, 1964

Sneden C., Kraft R. P., Guhathakurta P., Peterson R. C., Fulbright J. P., 2004, AJ, 127, 2162

Sobeck J. S., Ivans I. I., Simmerer J. A., Sneden C., Hoeflich P., Fulbright J. P., Kraft R. P., 2006, AJ, 131, 2949

Stetson P. B., Pancino E., 2008, PASP, 120, 1332

Travaglio C., Gallino R., Arnone E., Cowan J., Jordan F., Sneden C., 2004, ApJ, 601, 864

Ventura P., D'Antona F., 2009, A&A, 499, 835

Ventura P., Criscienzo M. D., D'Antona F., Vesperini E., Tailo M., Dell'Agli F., D'Ercole A., 2014, MNRAS, 437, 3274

Villanova S., Geisler D., 2011, A&A, 535, A31

Villanova S., Geisler D., Carraro G., Moni Bidin C., Muñoz C., 2013, ApJ, 778, 186

Yong D., Grundahl F., Nissen P. E., Jensen H. R., Lambert D. L., 2005, A&A, 438, 875

This paper has been typeset from a TEX/LATEX file prepared by the author.